Metal Dihydride (MH_2) and Dimer (M_2H_4) Structures in Solid Argon, Neon, and Hydrogen (M = Ca, Sr, and Ba): Infrared Spectra and Theoretical Calculations

Xuefeng Wang and Lester Andrews*

Department of Chemistry, University of Virginia, Charlottesville, Virginia 22901

Received: September 1, 2004; In Final Form: October 1, 2004

Laser-ablated Ca, Sr, and Ba atoms were co-deposited with H_2 in excess argon, neon, and hydrogen to form alkaline-earth metal hydrides. The metal dihydrides (CaH_2, SrH_2, and BaH_2) were identified in solid argon, neon, and hydrogen. Increasing infrared intensity in the symmetric stretching mode and electronic structure calculations show that these dihydride molecules have decreasing obtuse valence angles, respectively. These MH_2 molecules also form $(H_2)_nMH_2$ complexes. Further dimerization of metal dihydrides gave double-bridged $HCaH_2CaH$ with D_{2h} symmetry and triple-bridged $HSrH_3Sr$ and $HBaH_3Ba$ with C_{3v} symmetry, which are confirmed by D_2 and HD isotopic substitutions and quantum chemical calculations. Bonding in heavy alkaline metal hydrides is discussed.

Introduction

Solid-state CaH_2, SrH_2, and BaH_2 form orthorhombic structures,[1] but little is known about the molecular heavy alkaline-earth dihydrides.[2] The CaH_2 molecule was identified in solid xenon and krypton through photoexcited atomic calcium reacting with H_2;[3] however, searching for heavy alkaline-earth dihydrides in the gas phase was unsuccessful, since these molecules are less stable with respect to the metal atom and molecular hydrogen.[2] In contrast, the structures of heavy alkaline-earth dihydrides have been extensively studied theoretically and the computed results are not consistent with each other in some cases; the linear or bent structures for CaH_2 depend on different theoretical methods.[4−7] Similar to alkaline-earth dihalides, the bending potentials of alkaline-earth dihydrides are extremely shallow, resulting in variable bond angles from different computations.[8] Furthermore, the SrH_2 and BaH_2 molecules are predicted to be bent, which contradicts the expectations of the valence shell electron-pair repulsion (VSEPR) model for main-group structural chemistry.[4,5]

The diatomic hydrides are expected to be formed upon decomposition of the triatomic dihydrides. Indeed, a recent gas-phase investigation observed both CaH and SrH but not the dihydrides owing to their relative instability.[2]

Laser-ablated metal atom reactions with molecular hydrogen have been investigated extensively in our laboratory.[9] High-energy metal atoms generated by laser ablation react with H_2 during co-condensation in low-temperature matrixes. Some less stable molecules and reaction intermediates can be relaxed and trapped, and their molecular properties can be investigated. Annealing and photolysis promote further reaction to give higher-order metal hydrides and hydrogen complexes. With this method, the light alkaline-earth hydrides, BeH_2, Be_2H_4, MgH_2, and Mg_2H_4, have been synthesized in solid argon, neon, and hydrogen.[10,11] The group 13 metal hydrides have been also been investigated thoroughly and Al_2H_6 and In_2H_6 found to have diborane-like bridge-bonded structures.[12,13]

In this paper, we present our search for heavy alkaline-earth hydrides in low-temperature matrixes. Infrared spectra are employed to collect molecular vibrational information, and theoretical calculations are used to reproduce molecular spectroscopic and structural properties. We report the first experimental evidence for the SrH_2 and BaH_2 molecules.

Experimental and Computational Methods

Laser-ablated Ca, Sr, and Ba atom reactions with hydrogen in excess molecular hydrogen and neon and during condensation at 4 K and in argon at 8 K were performed as described in detail previously.[14,15] The Nd:YAG laser fundamental (1064 nm, 10 Hz repetition rate with 10 ns pulse width) was focused onto a rotating metal target (Johnson Matthey). Fresh metal targets were cut, washed with dry hexane, filed clean, and quickly placed in the vacuum chamber. Even so, trace oxide absorptions[16] were observed in the initial sample deposits. The laser energy was varied as low as possible to avoid forming metal clusters in the matrix samples (typical energy is ∼1−3 mJ/pulse for hydrogen and neon experiments and ∼5 mJ/pulse for argon experiments). Fourier transform infrared (FTIR) spectra were recorded at a resolution of 0.5 cm^{-1} on a Nicolet 750 instrument with a 0.1 cm^{-1} accuracy using an HgCdTe detector. An efficient converter was used to prepare parahydrogen and orthodeuterium.[17] Matrix samples were annealed at different temperatures and irradiated by a medium-pressure mercury arc lamp (Phillips, 175W) with the globe removed using optical filters for 20 min periods.

Complementary density functional theory (DFT) calculations were performed using the Gaussian 98 program,[18] the B3LYP density functional, and the 6-311++G(3df,3pd) basis for H and Ca and the SDD pseudopotential and basis for Sr and Ba. Additional MP2 calculations were done for comparison.

Results

Infrared spectra from laser-ablated Ca, Sr, and Ba atom co-condensation reactions with hydrogen in argon and neon and with pure hydrogen and calculations on the metal hydride products will be reported.

Calcium. Figure 1 illustrates the Ca−H stretching and Ca−D stretching regions from the infrared spectra of reaction products

* Corresponding author. E-mail: lsa@virginia.edu.

10.1021/jp046046m CCC: $27.50
Published on Web 12/07/2004

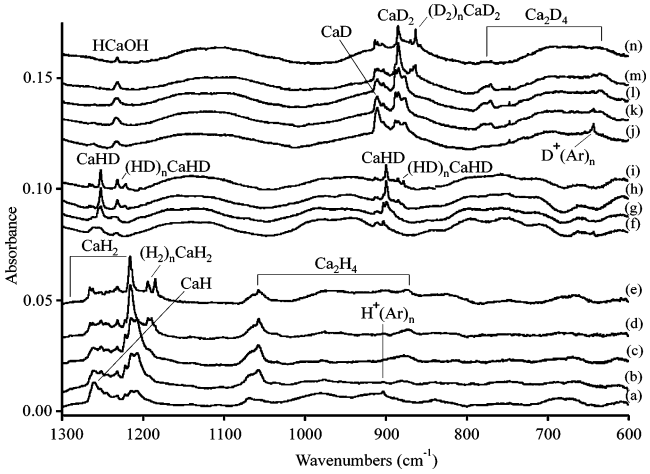

Figure 1. Infrared spectra in the 1300−600 cm^{-1} region for laser-ablated Ca reactions with hydrogen during deposition in excess argon at 8 K: (a) 4% H_2, deposited sample; (b) after $\lambda > 320$ nm irradiation; (c) after $\lambda > 290$ nm irradiation; (d) after annealing to 20 K; (e) after annealing to 27 K; (f) 4% HD, deposited sample; (g) after $\lambda > 290$ nm irradiation; (h) after annealing to 21 K; (i) after annealing to 27 K; (j) 4% D_2, deposited sample; (k) after $\lambda > 320$ nm irradiation; (l) after $\lambda > 290$ nm irradiation; (m) after annealing to 21 K; (n) after annealing to 31 K.

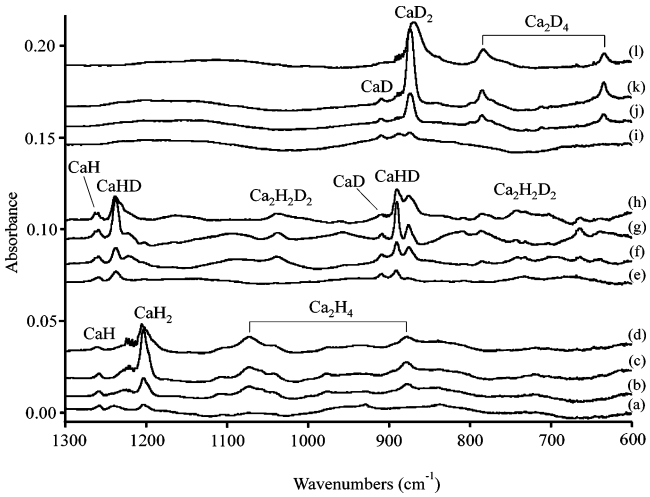

Figure 2. Infrared spectra in the 1300−600 cm^{-1} region for laser-ablated Ca reactions with hydrogen during deposition in excess neon at 4 K: (a) 4% H_2, deposited sample; (b) after $\lambda > 360$ nm irradiation; (c) after $\lambda > 290$ nm irradiation; (d) after annealing to 12 K; (e) 4% HD, deposited sample; (f) after $\lambda > 360$ nm irradiation; (g) after $\lambda > 290$ nm irradiation; (h) after annealing to 12 K; (i) 4% D_2, deposited sample; (j) after $\lambda > 360$ nm irradiation; (k) after $\lambda > 290$ nm irradiation; (l) after annealing to 12 K.

with hydrogen, deuterium, and deuterium hydride in excess argon during condensation at 8 K. Weak bands at 1262.0, 1232.4, 1216.3, 1057, and 874 cm^{-1} were observed with 4% H_2 in solid argon. No changes were observed for $\lambda > 530$ nm irradiation, but with $\lambda > 320$ nm photolysis, the 1216.3 and 1057, and 874 cm^{-1} bands increased, while the 1262.0 cm^{-1} band decreased, and further irradiation at $\lambda > 290$ nm continued these trends. A weak 1289.7 cm^{-1} band is associated with the stronger 1216.3 cm^{-1} absorption. The above bands decreased upon annealing, but new 1194.9 and 1186.3 cm^{-1} absorptions appeared. The 1232.4 cm^{-1} band has been assigned to HCaOH from the photochemical reaction of Ca and H_2O.[19a] With 4% D_2 in argon, these bands shift to 911.1, 884.9, 771, and 634 cm^{-1} and to 869.9 and 863.6 cm^{-1}, respectively. The HD spectra are illustrated between the H_2 and D_2 spectra for comparison and band identification, and the product absorptions are listed in Table 1. Weak absorptions were observed at 903 and 644 cm^{-1} for the Ar_nH^+ and Ar_nD^+ species.[19b]

The infrared spectra of Ca atom reactions with H_2, D_2, and HD in neon are shown in Figure 2. After deposition with H_2, weak bands appeared at 1258.2, 1240, and 1203.1 cm^{-1}. With $\lambda > 380$ nm photolysis, the 1203.1 cm^{-1} band increased 3-fold, the 1240 cm^{-1} band almost disappeared, and new bands appeared at 1221.0, 1072, and 878 cm^{-1}, while the 1258.2 cm^{-1} band did not change its intensity; $\lambda > 290$ nm irradiation increased the 1203.1 cm^{-1} another 3-fold. Upon annealing to 12 K, all bands decreased and a shoulder appeared at 1199 cm^{-1}. Experiments were done with pure normal H_2 (n-H_2), normal D_2 (n-D_2), parahydrogen (p-H_2), orthodeuterium (o-D_2), and HD, and the spectra in Figure 3 show that similar products were obtained. Our solid molecular hydrogen spectra contain perturbed H_2 absorptions common to all metals that have been described previously.[15] Similarly, weak absorptions due to $(H_2)_n$ trapped in solid argon at 4151 cm^{-1} and in solid neon at 4149 cm^{-1} and $(D_2)_n$ trapped in solid argon at 2985 cm^{-1} and in solid neon at 2982 cm^{-1} are common to these experiments.

Strontium. The major strontium hydride infrared spectra are shown in Figures 4−6, and the product absorptions are summarized in Table 2. With H_2 in argon, three bands were observed at 1202.1, 1174.6, and 1132.4 cm^{-1} upon deposition. Irradiation ($\lambda > 290$ nm) increased the 1202.1 and 1132.4 cm^{-1}

TABLE 1: Infrared Absorptions (cm^{-1}) Observed from Reactions of Calcium and Dihydrogen in Solid Pure Hydrogen, Neon, and Argon

n-H_2	p-H_2	n-D_2	o-D_2	HD	H_2/Ne	D_2/Ne	HD/Ne	H_2/Ar	HD/Ar	D_2/Ar	identification
4071	2920										$(H_2)_nCaH_2$
1257.5	1258.5	909.8	910.1	1259.9, 909.9	1258.2	908.9	1258.2, 908.9			914.9	CaH/CaD
1255.1	1256.6	907.6	907.9	1257.3, 908.2				1262.0		911.1	CaH/CaD
1251.9		904.1		1252.4, 904.7				1252.6		903.2	CaH/CaD
1215.4		877		1219.9, 872.8	1221.0	886.6	1222, 876				Ca_2H_4/Ca_2D_4
				1211.5, 867.8							
					1240	888					HCaCaH
								1289.7		(914.9)	CaH_2/CaD_2 (ν_1)
1196.9	1204.4	870.9	873.2	1203.7, 877.1	1203.1	873.7		1216.3		884.9	CaH_2/CaD_2 (ν_3)
				1237.9, 889.9			1234.4, 890.1		1253.0, 899.9		CaHD
1186.3	1196.0	866.8	869.7	1193.0, 869				1194.9		869.9	CaH_2/CaD_2 (site)
1183.9	1194.7	861.7	866.4	1190.5, 867.2				1186.3		863.6	CaH_2/CaD_2 (site)
				1229.1, 883.7					1232.6, 885.3		CaHD (site)
				1226.6, 882.0					1222.5, 878.4		$CaHD(HD)_y$
1073	1071	783	782	1161, 1034, 806	1072	785	1164, 1037, 808	1070	1031	779	Ca_2H_4/Ca_2D_4
				783, 740, 662			785, 742, 664	1057		771	Ca_2H_4/Ca_2D_4
877	876	631	632		878	634		874		634	Ca_2H_4/Ca_2D_4

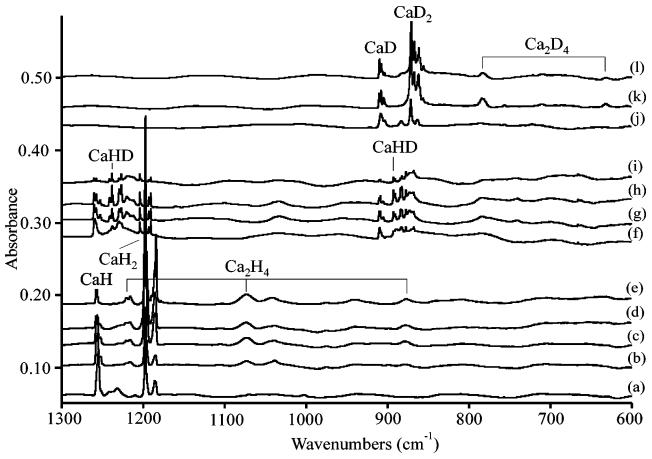

Figure 3. Infrared spectra in the 1300−600 cm^{-1} region for laser-ablated Ca reactions with hydrogen during deposition in pure hydrogen at 4 K: (a) H_2 deposited; (b) after $\lambda > 470$ nm irradiation; (c) after $\lambda > 360$ nm irradiation; (d) after $\lambda > 290$ nm irradiation; (e) after annealing to 7.2 K; (f) HD deposited; (g) after $\lambda > 360$ nm irradiation; (h) after $\lambda > 290$ nm irradiation; (i) after $\lambda > 220$ nm irradiation; (j) D_2 deposited; (k) after $\lambda > 290$ nm irradiation; (l) after annealing to 10 K.

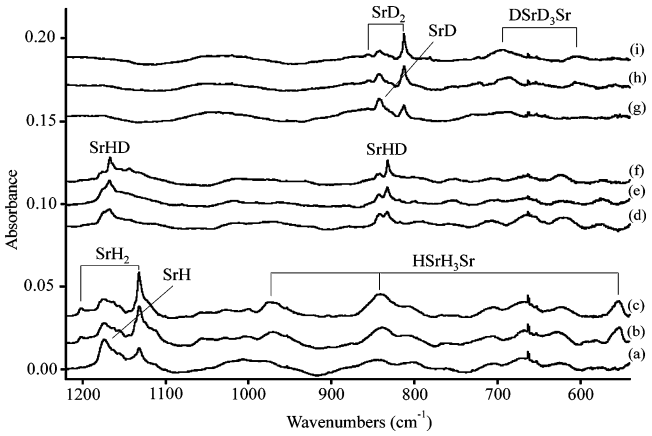

Figure 4. Infrared spectra in the 1220−540 cm^{-1} region for laser-ablated Sr reactions with hydrogen during deposition in excess argon at 8 K: (a) 4% H_2, deposited sample; (b) after $\lambda > 290$ nm irradiation; (c) after annealing to 17 K; (d) 4% HD, deposited sample; (e) after $\lambda > 290$ nm irradiation; (f) after annealing to 20 K; (g) 4% D_2, deposited sample; (h) after $\lambda > 290$ nm irradiation; (i) after annealing to 20 K.

bands 5-fold, while the 1174.6 cm^{-1} band decreased. Similar D_2 and HD argon matrix experiments were performed, and the spectra are shown in Figure 4. Our Sr atom reactions with H_2 in neon employed a very low ablation laser energy in order to avoid forming metal clusters upon deposition. As shown in Figure 5, the strontium hydride product absorptions are very weak upon deposition, but strong 1100.4 cm^{-1} and broad 979 cm^{-1} bands (H_2 experiment) and strong 788.8 and 718 cm^{-1} bands (D_2 experiment) were produced upon $\lambda > 290$ nm photolysis. Similar spectra with stronger bands are observed in pure H_2, D_2, *p*-H_2, and *o*-D_2 (Figure 6).

Barium. Laser-ablated Ba atom reactions with H_2 were also performed in argon, neon, and pure hydrogen. Infrared spectra of Ba−H and Ba−D stretching regions in solid argon are illustrated in Figure 7 for 6% H_2 samples. A weak band was observed at 1068.6 cm^{-1} upon deposition. Irradiation at $\lambda > 380$ nm increased this band 10-fold and produced new features at 1128.6, 1098.8, and 1036.4 cm^{-1}. Subsequent 240−380 nm irradiation decreased all absorptions. Annealing to 20 K formed a broad 1030 cm^{-1} band. The 1036−1030 cm^{-1} absorption was

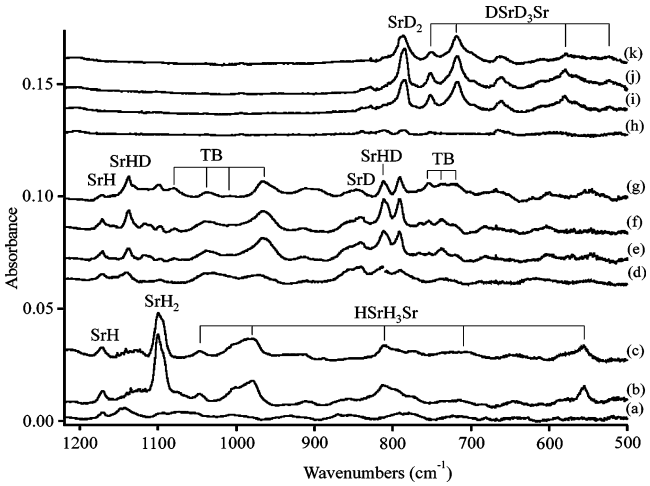

Figure 5. Infrared spectra in the 1220−500 cm^{-1} region for laser-ablated Sr reactions with hydrogen during deposition in excess neon at 4 K: (a) 4% H_2, deposited sample; (b) after $\lambda > 290$ nm irradiation; (c) after annealing to 12 K; (d) 4% HD; (e) after $\lambda > 360$ nm irradiation; (f) after $\lambda > 290$ nm irradiation; (g) after annealing to 11 K; (h) 4% D_2; (i) after $\lambda > 360$ nm irradiation; (j) after $\lambda > 290$ nm irradiation; (k) after annealing to 13 K. TB denotes triple-bridged $Sr_2H_2D_2$.

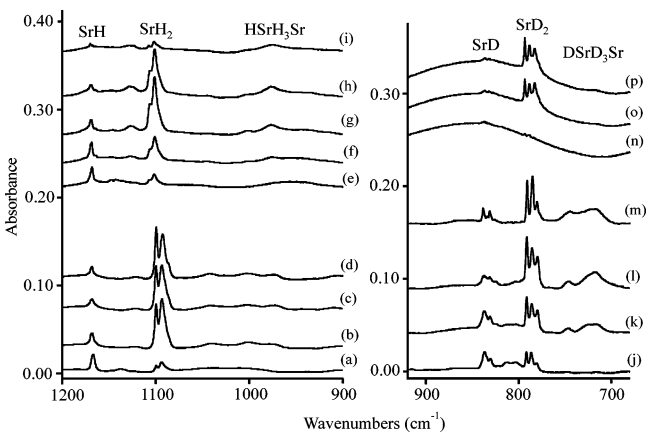

Figure 6. Infrared spectra in the 1200−900 and 920−680 cm^{-1} regions for laser-ablated Sr reactions with hydrogen during deposition in pure hydrogen at 4 K: (a) *n*-H_2 deposited; (b) after $\lambda > 360$ nm irradiation; (c) after $\lambda > 290$ nm irradiation; (d) after annealing to 6.8 K; (e) *p*-H_2 deposited; (f) after $\lambda > 420$ nm irradiation; (g) after $\lambda > 360$ nm irradiation; (h) after $\lambda > 290$ nm irradiation; (i) after $\lambda > 220$ nm irradiation; (j) *n*-D_2 deposited; (k) after $\lambda > 360$ nm irradiation; (l) after $\lambda > 290$ nm irradiation; (m) after annealing to 10 K; (n) *o*-D_2 deposited; (o) after $\lambda > 360$ nm irradiation; (p) after $\lambda > 290$ nm irradiation.

much weaker relative to the 1068.6 cm^{-1} band in samples with 2% H_2. Experiments with a higher laser energy, 4% H_2, and a 12 K substrate gave a sharp 1132.5 cm^{-1} feature on the side of the 1128.6 cm^{-1} absorption and broad 875 and 745 cm^{-1} bands, but the 1068.6 cm^{-1} band was still dominant. The product absorptions shifted with HD and D_2, as shown in Figure 7 and listed in Table 3. With higher laser energy and 4% D_2 in excess argon, a sharp 809.9 cm^{-1} shoulder was observed on the 803.7 cm^{-1} band and broad 627 and 535 cm^{-1} bands were also observed. With HD, the 1098.0 and 782.5 cm^{-1} bands were dominant but the same absorptions were observed at 1132.5 and 809.9 cm^{-1} along with broad features at 887, 860 cm^{-1} and 686, 664 cm^{-1}.

The behavior of the Ba and H_2 reaction in excess neon was somewhat different: Very weak features at 1027.6 and 881.0 cm^{-1} upon sample deposition increased upon $\lambda > 380$ nm irradiation, and sharp 1131.3 and 1067.9 cm^{-1} bands were

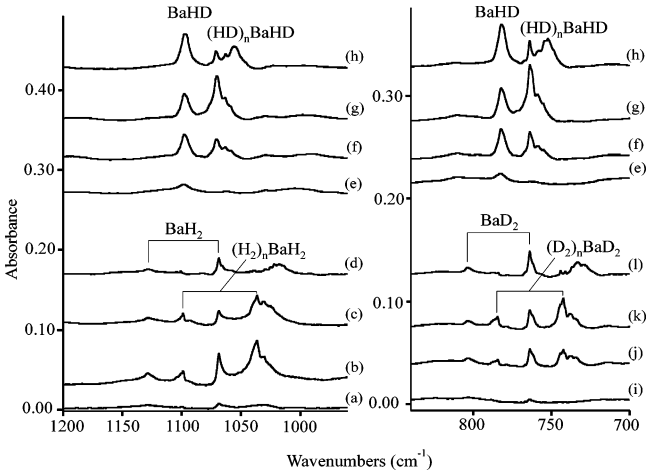

Figure 7. Infrared spectra in the 1200−960 and 840−700 cm^{-1} regions for laser-ablated Ba reactions with hydrogen during co-deposition in excess argon at 8 K: (a) 6% H_2, deposited sample; (b) after $\lambda > 360$ nm irradiation; (c) after 240−380 nm irradiation; (d) after annealing to 20 K; (e) 6% HD, deposited sample; (f) after $\lambda > 360$ nm irradiation; (g) after $\lambda > 320$ nm irradiation; (h) after annealing to 17 K; (i) 6% D_2, deposited sample; (j) after $\lambda > 360$ nm irradiation; (k) after $\lambda > 320$ nm irradiation; (l) after annealing to 18 K.

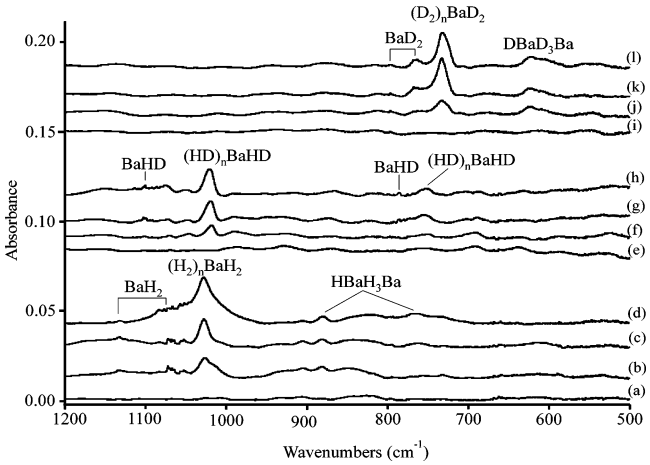

Figure 8. Infrared spectra in the 1200−500 region for laser-ablated Ba reactions with hydrogen during co-deposition in excess neon at 4 K: (a) 4% H_2, deposited sample; (b) after $\lambda > 360$ nm irradiation; (c) after 240−380 nm irradiation; (d) after annealing to 9 K; (e) 4% HD, deposited sample; (f) after $\lambda > 360$ nm irradiation; (g) after $\lambda > 320$ nm irradiation; (h) after annealing to 9 K; (i) 4% D_2, deposited sample; (j) after $\lambda > 360$ nm irradiation; (k) after 240−380 nm irradiation; (l) after annealing to 9 K.

produced (Figure 8). Further, 240−380 nm irradiation slightly increased the broader bands. Analogous results were obtained for D_2, but a new band formed with HD at 1019 cm^{-1}. This behavior carried over to the solid molecular hydrogens (Figure 9) where strong 1064.6, 1007.6, and 874.4 cm^{-1} bands were produced in H_2, and their counterparts in D_2, but only a weak 1024.5, 1014.4 cm^{-1} band was observed in solid HD.

Calculations. Systematic calculations were performed on the MH and MH_2 molecules and several dimer structures to provide a consistent set of infrared intensities and frequencies for H, D, and mixed H/D isotopic molecules to aid in making vibrational assignments following the work of Kaupp et al.[4,20] Tables 4, 5, and 6 summarize the results for calcium, strontium, and barium hydrides, respectively.

TABLE 2: Infrared Absorptions (cm^{-1}) Observed from Reactions of Strontium with Dihydrogen in Solid Pure Hydrogen, Neon, and Argon

n-H_2	*p*-H_2	*n*-D_2	*o*-D_2	H_2/Ne	D_2/Ne	HD/Ne	H_2/Ar	HD/Ar	D_2/Ar	identification
4090		2940			2915					$(H_2)_nSrH_2$
4060		2912		4052	2899					$(H_2)_nSrH_2$
1168.3	1170.2	836.8	836.5	1171.5	839.3	1171.5, 839.3	1174.6	1174.6, 842.7	842.7	SrH/SrD
1166.7	1168.3	831.2	832.2							SrH/SrD (site)
	1126.4						1202.1	1167.0	855.0	SrH_2/SrD_2
1121				1125	810					$HSrH_3Sr/DSrD_3Sr$
1099.5	1106.6	791.4	793.5	1100.4	788.8	1137.7, 811.1	1132.4	832.7	812.9	SrH_2/SrD_2
1093.5		785.5	788.3	1093						SrH_2/SrD_2 (site)
1086	1101.1	779.9	782.7							SrH_2/SrD_2 (site)
1041		747	715.9	1047	752	1079, 1038		1020		$HSrH_3Sr/DSrD_3Sr$
974	977	717		979	718	967	975		693	$HSrH_3Sr/DSrD_3Sr$
808	810	577		813	581	755	839	751, 707	602	$HSrH_3Sr/DSrD_3Sr$
				719	521	738, 720				$HSrH_3Sr/DSrD_3Sr$
556			556	556			553			$HSrH_3Sr/DSrD_3Sr$

TABLE 3: Infrared Absorptions (cm^{-1}) Observed from Reactions of Barium with Dihydrogen in Solid Pure Hydrogen, Neon, and Argon

n-H_2	*n*-D_2	H_2/Ne	HD/Ne	D_2/Ne	H_2/Ar	HD/Ar	D_2/Ar	identification
4042	2903	4042	3531	2902				$(H_2)_nBaH_2$
3966	2852	3976	3458	2850				$(H_2)_nBaH_2$
		1131.3	1100.4		1128.6	1098.0		BaH_2
				807.7			803.7	BaD_2
					1132.5	1132.5		BaH
						809.9	809.9	BaD
1064.6					1098.8			$(H_2)_nBaH_2$
	764.2						784.4	$(D_2)_nBaD_2$
		1067.9	785.5		1068.6	782.5		BaH_2
				764.9			764.0	BaD_2
1007.6			1019.5		1036.4	1070.6		$(H_2)_nBaH_2$
	727.3		750			764.0	742.5	$(D_2)_nBaD_2$
		1027.6	1050	732.7	1030		733	$(H_2)_nBaH_2$
								$HBaH_3Ba/DBaD_3Ba$
874	620	881		626	875	887, 860	627	$HBaH_3Ba/DBaD_3Ba$
730	560	758			745	686, 664	535	$HBaH_3Ba/DBaD_3Ba$

TABLE 4: Calculations of Calcium Hydrides at the B3LYP and MP2 Levels of Theory with the 6-311++G(3df,3pd) Basis Set

species	geometry[a]	rel energy[b]	frequencies, cm^{-1} (intensities, km/mol)[c]
			B3LYP
CaH ($^2\Sigma$)	Ca−H: 1.985		**CaH**: 1292.9 (332); **CaD**: 925.7 (170)
CaH_2 ($^1A_1$)	CaH: 2.030 HCaH: 142.7		**CaH_2**: 1333.4 (a_1, 35), 1261.3 (b_2, 923), 216.9 (a_1, 665) **CaD_2**: 946.5 (20), 911.3 (486), 156.6 (346) **CaHD**: 1299.0 (428), 927.4 (305), 189.2 (511)
HCaCaH ($^1\Sigma_g$)	CaH: 2.008 CaCa: 3.800	0.0	**HCaCaH**: 1296.5 (σ_g, 0), 1286.5 (σ_u, 1930), 137.2 (σ_g, 0), 93.7 (π_g, 0 × 2), 88.3 (π_u, 413 × 2)
$CaCaH_2$ ($^1A_1$)	CaCa: 4.134 CaH: 2.035 HCaH: 135.4	3.7	**$CaCaH_2$**: 1290.9 (a_1, 287), 1220.5 (b_2, 744), 316.6 (a_1, 670), 122.4 (b_1, 590), 73.6 (a_1, 0), 13.3 (b_2, 25)
$HCaH_3Ca$ ($^1A_1$) (C_{3v})	CaH: 2.041 CaH′: 2.295 Ca′H′: 2.076	0.0	**$HCaH_3Ca$**: 1257.5 (a_1, 621), 1217.4 (a_1, 191), 1094.6 (e, 537 × 2), 902.0 (a_1, 981), 716.2 (e, 75 × 2), 611.2 (e, 466 × 2), 256.5 (a_1, 1), 240.2 (e, 249 × 2) **$DCaD_3Ca$**: 899.4 (359), 870.9 (102), 782.2 (289 × 2), 645.8 (477), 510.6 (47 × 2), 437.6 (236 × 2), 253.7 (1), 175.5 (115 × 2) **$HCaHD_2Ca$**: 1252.9 (605), 1142.7 (365), 849.4 (620), 789.5 (260), 782.8 (314), 573.4 (159), 572.3 (186), ... **$DCaH_2DCa$**: 1183.5 (359), 1094.2 (519), 919.7 (19), 849.4 (1058), 795.6 (209), 710.7 (145), 623.8 (225), ...
Ca_2H_4 (^1A_g) (D_{2h})	CaH: 2.025 CaH′: 2.198 CaH′Ca: 102.5	1.2	**Ca_2H_4**: 1306.2 (a_g, 0), 1291.6 (b_{1u}, 686), 1087.9 (b_{1u}, 1999), 981.0 (a_g, 0), 960.3 (b_{3g}, 0), 900.3 (b_{2u}, 823), 481.2 (b_{3u}, 646), 248.2 (b_{3g}, 0), 222.3 (b_{2u}, 546), 204.9 (a_g, 0), 77.8 (b_{3u}, 747), 23.8 (b_{2g}, 0) **Ca_2D_4**: 934.3 (0), 920.6 (445), 781.8 (963), 697.8 (0), 685.2 (0), 646.4 (441), ... **HCaHDCaD**: 1295.6 (456), 1041.1 (822), 957.6 (431), 910.3 (421), 723.2 (235), 669.6 (319), 419.1 (498), ...
			MP2
CaH ($^2\Sigma$)	CaH: 2.002		**CaH**: 1307.2 (453); **CaD**: 936.0 (232)
HCaH ($^1\Sigma_g$)	CaH: 2.044 HCaH: 180.0		**CaH_2**: 1350.2 (σ_g, 0), 1264.0 (σ_u, 953), 89.1 (π_u, 953 × 2) **CaD_2**: 955.1 (0), 915.3 (500), 64.5 (500 × 2) **CaHD**: 1309.7 (421), 932.8 (305), 77.8 (726 × 2)
$HCaH_3Ca$ ($^1A_1$) (C_{3v})	CaH: 2.043 CaH′: 2.302 Ca′H′: 2.075	0.0	**$HCaH_3Ca$**: 1276.9 (a_1, 581), 1233.4 (a_1, 347), 1112.7 (e, 553 × 2), 917.9 (a_1, 1134), 722.5 (e, 47 × 2), 635.3 (e, 632 × 2), 266.6 (a_1, 0), 245.6 (e, 286 × 2) **$DCaD_3Ca$**: 913.4 (346), 882.1 (183), 795.1 (300), 656.8 (552), 514.2 (32 × 2), 455.5 (322 × 2), 263.9 (0), 179.6 (132 × 2)
Ca_2H_4 (^1A_g) (D_{2h})	CaH: 2.028 CaH′: 2.194 CaH′Ca: 103.4	−1.4	**Ca_2H_4**: 1324.6 (a_g, 0), 1312.9 (b_{1u}, 584), 1126.3 (b_{1u}, 2001), 1021.3 (a_g, 0), 1013.7 (b_{3g}, 0), 910.3 (b_{2u}, 920), 518.0 (b_{3u}, 793), 245.8 (b_{3g}, 0), 228.8 (b_{2u}, 652), 215.1 (a_g, 0), 123.7 (b_{3u}, 714), 115.2 (b_{2g}, 0)

[a] Bond lengths (angstroms) and bond angles (degrees). [b] Relative energy in kilocalories per mole. [c] Frequencies not scaled.

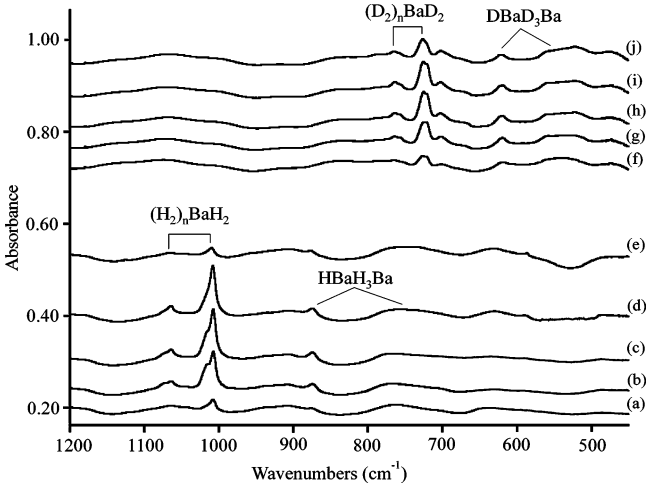

Figure 9. Infrared spectra in the 1200−450 cm^{-1} region for laser-ablated Ba reactions with hydrogen during co-deposition in pure hydrogen at 4 K: (a) *n*-H_2 deposited; (b) after $\lambda > 470$ nm irradiation; (c) after $\lambda > 420$ nm irradiation; (d) after $\lambda > 290$ nm irradiation; (e) after $\lambda > 220$ nm irradiation; (f) *n*-D_2 deposited; (g) after $\lambda > 470$ nm irradiation; (h) after $\lambda > 360$ nm irradiation; (i) after $\lambda > 290$ nm irradiation; (j) after $\lambda > 220$ nm irradiation.

Discussion

The heavy group 2 hydride products will be identified by deuterium substitution and by comparison with computed isotopic frequencies.

CaH, SrH, and BaH. The group 2 diatomic hydrides have been investigated in the gas phase,[21] and recent high-resolution work has provided accurate vibrational frequencies.[2,22−26] These diatomic hydrides are expected from the decomposition of the dihydride molecules formed in the reaction of laser-ablated metal atoms with dihydrogen.[24] A band at 1262.0 cm^{-1} appeared after the initial deposition of Ca with H_2 in argon and decreased upon near-UV photolysis and annealing to 20 K. The D_2 counterpart at 911.1 cm^{-1} gives a 1.385 H/D isotopic ratio. The HD experiment reveals an isotopic doublet at 1262.0 and 911.1 cm^{-1}, suggesting assignment to the diatomic molecule CaH. In solid neon, CaH absorption appeared at 1258.2 cm^{-1} and CaD absorption at 908.9 cm^{-1}. Again, the doublet at 1258.2 and 908.9 cm^{-1} in the HD experiment in neon confirms that a single H(D) atom is involved. The CaH and CaD molecules were also trapped in solid hydrogen (1255.1 cm^{-1}) and deuterium (904.1 cm^{-1}) (*p*-H_2 and *o*-D_2, see Table 1). The absorptions of CaH in solid neon and hydrogen are 1.8 and 4.9 cm^{-1}, respectively, below the gas-phase fundamental[2] at 1260.0 cm^{-1}, which is excellent agreement. However, the argon value is 2.0 cm^{-1} higher, suggesting a strong interaction between argon and calcium where the Ca atom is partly polarized. Although argon matrix blue shifts are not common, they have been observed for coinage metal hydrides.[9]

The absorption of SrH was observed at 1171.5 cm^{-1} in neon, 1166.7 cm^{-1} in hydrogen, and 1174.6 cm^{-1} in argon upon deposition. With D_2, these bands shift to 839.3, 836.8, and 842.5 cm^{-1}, respectively. With HD, the same two bands were observed

TABLE 5: Calculations of Strontium Hydrides at the B3LYP and MP2 Levels of Theory

species	geometry[a]	rel energy[b]	frequencies, cm^{-1} (intensities, km/mol)[c]
			B3LYP/6-311++G(3df,3pd)/SDD
SrH ($^2\Sigma$)	Sr−H: 2.143		**SrH**: 1184.2 (323); **SrD**: 842.4 (164)
SrH_2 ($^1A_1$)	SrH: 2.164		**SrH_2**: 1227.6 (a_1, 117), 1159.9 (b_2, 906), 343.6 (a_1, 309)
	HSrH: 124.5		**SrD_2**: 871.3 (61), 827.7 (465), 244.9 (157)
			SrHD: 1195.5 (454), 848.1 (322), 298.6 (245)
$SrH_2Sr(^1A_1)$ (D_{2h})	SrH: 2.340 SrSr: 3.809	0.0	**SrH_2Sr**: 933.0 (a_g, 0), 931.5 (b_{3g}, 0), 809.7 (b_{1u}, 2111), 762.3 (b_{2u}, 264), 456.9 (b_{3u}, 70), 140.5 (a_g, 0)
SrHSrH ($^1A'$) (C_s)	SrSr: 3.727 SrH: 2.372 Sr′H: 2.283 Sr′H′: 2.174	3.4	**SrHSrH**: 1178.7(a′, 1221), 973.2 (a′, 29), 786.6 (a′, 438), 203.8 (a′, 259), 94.8 (a′, 17), 68.6 (a″, 310)
$SrSrH_2$ ($^1A_1$) (C_{2v})	SrSr: 4.576 SrH: 2.184 HSrH: 124.6	14.7	**$SrSrH_2$**: 1187.0 (a_1, 471), 1122.6 (b_2, 769), 346.8 (a_1, 331), 89.2 (b_1, 640), 72.4 (b_2, 75), 44.8 (a_1,0)
$HSrH_3Sr$ ($^1A_1$) (C_{3v})	SrH: 2.212 SrH′: 2.465 Sr′H′: 2.234	0.0	**$HSrH_3Sr$**: 1142.9 (a_1, 804), 1111.1 (a_1, 201), 1003.5 (e, 586 × 2), 827.3 (a_1, 956), 675.6 (e, 102 × 2), 553.2 (e, 444 × 2), 209.7 (e, 263 × 2), 159.1 (a_1, 0) **$DSrD_3Sr$**: 812.5(433), 790.3(99), 713.1(303 × 2), 588.6(471), 479.9(56 × 2), 393.5(223 × 2), 158.2(0), 150.7(127 × 2)
Sr_2H_4 (^1A_g) (C_{2h})	SrH: 2.176 SrH′: 2.348 CaH′Ca: 104.6	4.9	**Sr_2H_4**: 1191.8 (a_g, 0), 1185.9 (b_u, 651), 1029.2 (b_u, 2173), 910.1 (b_g, 0), 905.8 (a_g, 0), 817.7 (a_u, 921), 469.8 (b_u, 525), 338.4 (b_g, 0), 235.5 (a_u, 514), 173.0 (a_g, 0), 126.8 (a_g, 0), 122.0 (b_u, 532)
			MP2/6-311++G(3df,3pd)/SDD
SrH ($^2\Sigma$)	Sr−H: 2.161		**SrH**: 1179.2 (464); **SrD**: 838.8 (235)
SrH_2	SrH: 2.194		**SrH_2**: 1227.6 (a_1, 76), 1141.4 (b_2, 1053), 233.4 (a_1, 704)
	HSrH: 140.1		**SrD_2**: 870.1 (40), 815.3 (540), 166.6 (358)
			SrHD: 1187.6 (481), 839.9 (374), 202.6 (539)
$HSrH_3Sr$ ($^1A_1$) (C_{3v})	SrH: 2.223 SrH′: 2.474 Sr′H′: 2.238	0.0	**$HSrH_3Sr$**: 1154.7 (a_1, 687), 1125.5 (a_1, 444), 1014.5 (e, 613 × 2), 855.9 (a_1, 1164), 691.1 (e, 159 × 2), 570.1 (e, 567 × 2), 222.3 (e, 304 × 2), 165.7 (a_1, 0)
Sr_2H_4 (^1A_g) (C_{2h})	SrH: 2.207 SrH′: 2.376 HSrH′: 142.1 SrH′Sr: 104.5	3.8	**Sr_2H_4**: 1195.3 (a_g, 0), 1182.0 (b_u, 473), 1021.5 (b_u, 2389), 928.0 (b_g, 0), 912.8 (a_g, 0), 838.5 (a_u, 993), 448.4 (b_u, 791), 222.1 (b_g, 0), 197.3 (a_u, 662), 130.2 (a_g, 0), 85.6 (b_u, 884), 28.1 (a_g, 0)

[a] Bond lengths (angstroms) and bond angles (degrees). [b] Relative energy in kilocalories per mole. [c] Frequencies not scaled.

in each experiment, which confirms the diatomic SrH assignment. Our observation of SrH is in very good agreement with the gas-phase 1172.8 cm^{-1} fundamental frequency.[2] Again, the argon value is slightly higher, suggesting a strong interaction between argon and the strontium center.

In slightly higher laser energy experiments, diatomic BaH gives a band at 1132.5 cm^{-1} in solid argon with a BaD counterpart at 809.9 cm^{-1} (H/D ratio 1.398) and the HD reagent provides the same bands. Unfortunately, we cannot identify BaH and BaD in solid neon and hydrogen. Our argon matrix value (1132.5 cm^{-1}) is slightly red-shifted from the 1139.2 cm^{-1} gas-phase observation,[26] which is the more typical relationship.[27]

Vibrational assignments of CaH, SrH, and BaH are in agreement with our theoretical calculations. At the B3LYP level, the M−H stretching frequencies are predicted to be 1292.9 cm^{-1} for CaH, 1184.2 cm^{-1} for SrH, and 1155.4 cm^{-1} for BaH, which gives overestimations of 2.6% for CaH, 1.0% for SrH, and 1.4% for BaH in comparison with gas-phase values, which is excellent agreement and in line with other observations.[9,28]

The broad 1240 cm^{-1} band with Ca and H_2 in excess neon exhibits the photochemical behavior previously observed for HCaCaH. Our calculations verify the linear global minimum energy species and the H/D isotopic patterns reported by the Rice group[3] for this molecule. The low yields of SrH and BaH in these experiments precluded observation of their dimers.

CaH_2, SrH_2, and BaH_2. Two bands at 1289.7 and 1216.3 cm^{-1} tracked together upon near-UV irradiation of Ca with H_2 in solid argon, sharpened upon annealing to 20 K, and decreased upon annealing to 34 K. The deuterium counterparts at 914.9 cm^{-1} (estimated from the CaHD band at 899.9 cm^{-1}) and 884.9 cm^{-1} define 1.409 and 1.374 H/D isotopic frequency ratios. With HD in argon, two precise median bands at 1253.0 cm^{-1} (Ca−H stretching region) and 899.9 cm^{-1} (Ca−D stretching region) were obtained. This evidence confirms assignment of the 1289.7 and 1216.3 cm^{-1} bands to the symmetric (ν_1, a_1) and antisymmetric (ν_3, b_2) vibrational modes for CaH_2.[29] The B3LYP calculated CaH_2/CaD_2 harmonic frequency ratios for ν_1 and ν_3 are 1.409 and 1.384, respectively. It appears that there is more anharmonicity in the ν_3 mode than in the ν_1 mode. Note also that the calculated CaHD frequencies are 1.6 cm^{-1} above and 1.5 cm^{-1} below the average CaH_2 and CaD_2 mode values, respectively. The argon matrix CaH_2 frequencies observed here (1289.7 and 1216.3 cm^{-1}) are higher than the values reported for CaH_2 in the more polarizable and strongly interacting krypton (1267.0 and 1192.0 cm^{-1}) and xenon (1239.8 and 1163.8 cm^{-1}) matrix hosts,[3] as expected,[27] and our results support the earlier assignment. The large argon, krypton, and xenon matrix shifts observed for CaH_2 show how sensitive this molecule is to interaction even with different noble gas atoms. The H/D ratios for the ν_3 mode, however, are essentially the same (1.374 ± 0.001) in solid argon, krypton, and xenon, and the weak observed symmetric stretching modes argue for slightly bent structures in these three matrix environments.

The ν_3 mode of CaH_2 was observed at 1196.9 cm^{-1} in solid normal hydrogen, and that of CaD_2 was observed at 870.9 cm^{-1} in solid normal deuterium (H/D ratio 1.374). The solid HD sample revealed new sharp bands at 1237.9 cm^{-1} in the Ca−H stretching region and at 892.1 cm^{-1} in the Ca−D stretching region as well as sharp bands due to CaH_2 (1203.7 cm^{-1}) and CaD_2 (877.1 cm^{-1}, H/D ratio 1.372) (Figure 3). The ν_3 CaH_2 absorption (1204.4 cm^{-1}) in *p*-H_2 shifted to 873.2 cm^{-1} for CaD_2 in *o*-D_2 (ratio 1.379). Note that CaH_2 exhibits slightly different

TABLE 6: Calculations of Barium Hydrides at the B3LYP and MP2 Levels of Theory

species	geometry[a]	rel energy[b]	frequencies, cm^{-1} (intensities, km/mol)[c]
			B3LYP/6-311++G(3df,3pd)/SDD
BaH ($^2\Sigma$)	BaH: 2.252		**BaH**: 1155.4 (488); **BaD**: 820.3 (246)
BaH_2 ($^1A_1$)	BaH: 2.287		**BaH_2**: 1166.6 (a_1, 347), 1102.1 (b_2, 1167), 389.9 (a_1, 166)
	HBaH: 113.1		**BaD_2**: 827.5 (176), 783.5 (593), 277.0 (84)
			BaHD: 1136.3 (695), 803.8 (449), 338.6 (140)
$BaBaH_2$ ($^1A_1$)	BaBa: 5.113		**$BaBaH_2$**: 1129.7 (a_1, 1031), 1069.5 (b_2, 960), 384.5 (a_1, 109), 81.7 (b_1, 111),
(C_{2v})	BaH: 2.308		28.4 (a_1, 0), 62.1i (b_1, 617)
	HBaH: 114.3		
$HBaH_3Ba$ ($^1A_1$)	BaH: 2.371	0.0	**$HBaH_3Ba$**: 1052.0 (a_1, 1419), 1038.1 (a_1, 97), 925.5 (e, 714 × 2), 771.3 (a_1, 1059),
(C_{3v})	BaH′: 2.632		658.7 (e, 180 × 2), 467.4 (e, 278 × 2), 173.3 (e, 272 × 2), 107.8 (a_1, 1)
	Ba′H′: 2.394		**$DBaD_3Ba$**: 746.6 (755), 737.3 (28), 656.7 (364 × 2), 547.9 (522), 467.7 (92 × 2),
			331.5 (140 × 2), 123.9 (133 × 2), 107.3 (1)
			$HBaHD_2Ba$: 1041.8 (1062), 968.8 (502), 739.9 (991), 673.9 (62), 657.5 (405), 515.5 (274), ...
			$DBaH_2DBa$: 1007.8 (685), 924.9 (682), 799.0 (101), 706.6 (1143), 662.6 (280), 655.6 (165), ...
BaH_4Ba (^1A_g)	BaH: 2.458	4.5	**BaH_4Ba:** 958.0 (a_{1g}, 0), 944.1 (a_{2u}, 1380), 834.6 (e_u, 1423 × 2), 807.8 (b_{1g}, 0), 731.1 (b_{2g}, 0),
(D_{4h})	HBaH: 64.0		668.9 (e_g, 0 × 2), 662.7 (b_{2u}, 0), 584.1 (e_u, 211 × 2), 145.7 (a_{1g}, 0)
			MP2/6-311++G(3df,3pd)/SDD
BaH ($^2\Sigma$)	BaH: 2.244		**BaH**: 1167.4 (546); **BaD**: 828.8 (275)
BaH_2 ($^1A_1$)	BaH: 2.287		**BaH_2**: 1171.2 (a_1, 404), 1101.3 (b_2, 1552), 369.0 (a_1, 310)
	HBaH: 118.7		**BaD_2**: 830.6 (206), 783.2 (789), 262.2 (156)
			BaHD: 1138.3 (882), 805.2 (597), 319.8 (249)
$BaBaH_2$ ($^1A_1$)	BaBa: 5.067		**$BaBaH_2$**: 1134.2 (a_1, 1091), 1068.1 (b_2, 1243), 363.8 (a_1, 304), 54.8 (b_1, 747),
(C_{2v})	BaH: 2.309		33.4 (a_1, 0), 27.6 (b_1, 110)
	HBaH: 119.6		
$HBaH_3Ba$ ($^1A_1$)	BaH: 2.374	0.0	**$HBaH_3Ba$**: 1059.9 (a_1, 917), 1055.0 (a_1, 973), 934.3 (e, 789 × 2), 775.3 (a_1, 1165),
(C_{3v})	BaH′: 2.627		676.7 (e, 295 × 2), 488.0 (e, 348 × 2), 186.9 (e, 312 × 2), 113.8 (a_1, 1)
	Ba′H′: 2.378		**$DBaD_3Ba$**: 753.3 (558), 748.2 (418), 662.9 (403 × 2), 550.7 (575), 480.3 (151 × 2),
			346.1 (174 × 2), 133.5 (153 × 2), 113.3 (1)
BaH_4Ba (^1A_g)	BaH: 2.437	4.8	**BaH_4Ba**: 982.7 (a_{1g}, 0), 966.4 (a_{2u}, 1768), 850.7 (e_u, 1732 × 2), 841.0 (b_{1g}, 0), 766.1 (b_{2g}, 0),
(D_{4h})	BaHBa: 83.3		693.7 (b_{2u}, 0), 693.1 (e_g, 0 × 2), 608.9 (e_u, 246 × 2), 151.9 (a_{1g}, 0)

[a] Bond lengths (angstroms) and bond angles (degrees). [b] Relative energy in kilocalories per mole. [c] Frequencies not scaled.

absorptions in solid *n*-H_2, and HD as does CaD_2 in *n*-D_2, *o*-D_2, and HD. The ν_3 mode of CaH_2 was observed at 1203.1 cm^{-1} in solid neon, which shifts to 873.7 cm^{-1} upon D_2 substitution, exhibiting a 1.377 H/D isotopic ratio. With HD, the spectrum gave strong new bands at 1237.4 cm^{-1} in the Ca−H stretching region and at 873.7 cm^{-1} in the Ca−D region, which are due to the CaHD molecule. However, the ν_1 mode was not detected in solid neon or hydrogen, indicating a different interaction of CaH_2 with the lighter host matrixes that results in a more nearly linear CaH_2 structure. The H/D ratios can in principle reveal a trend in the H−Ca−H bond angle[29] if the anharmonicities are the same in the different matrixes. Unfortunately, we have no way to determine the anharmonicity for the ν_3 mode in these matrixes. Finally, in solid hydrogen, CaH_2 is weakly complexed to a number of H_2 "ligands", and this can also affect the CaH_2 subunit structure.

Upon annealing in solid argon, the decrease in CaH_2 absorption is accompanied first by an increase of a new band at 1194.9 cm^{-1} and then at 1186.3 cm^{-1} and the latter is dominant at the highest annealing. These H/D frequency ratios (1.374) and HD counterparts identify another CaH_2 species. The appearance of these bands near the hydrogen matrix 1196.9 cm^{-1} band, which involves some number of H_2 ligands, suggests the following sequence as H_2 replaces Ar in the coordination sphere around the Ca center: $(Ar)_nCaH_2$, $(Ar)_{n-1}(H_2)CaH_2$, and $(Ar)_{n-2}(H_2)_2CaH_2$.

The absorptions due to SrH_2 are identified at 1202.1 (ν_1) and 1132.4 (ν_3) cm^{-1} upon the deposition of laser-ablated Sr atoms with H_2 in solid argon. Upon $\lambda > 290$ nm photolysis, these two bands increased 5-fold. With D_2 in argon, these bands shifted to 855.0 and 812.9 cm^{-1}, giving 1.406 and 1.393 H/D isotopic ratios. The median bands at 1167.0 and 832.7 cm^{-1} in HD experiments are assigned to Sr−H and Sr−D stretching vibrations in the SrHD molecule. Similar spectra were observed for SrH_2 in solid neon and pure hydrogen as compared to those found for CaH_2 (see Figures 5 and 6). The ν_3 mode of SrH_2 was observed split at 1099.5, 1093.5 cm^{-1} in solid hydrogen and split at 1100.4, 1092.8 cm^{-1} in solid neon; however, the ν_1 mode was too weak to be detected. The absorption of SrH_2 in solid argon exhibits a striking difference: the ν_3 mode is ~32 cm^{-1} higher in argon, which is an unusual matrix shift for metal hydrides isolated in solid matrixes. In most cases, the infrared frequencies of metal hydrides observed in neon are slightly lower than the gas-phase value, but higher than in solid hydrogen and higher than in solid argon.[9]

Similar metal dihydride bands were observed for BaH_2 in solid argon. Two new bands at 1128.6 and 1068.6 cm^{-1} increased upon $\lambda > 380$ nm photolysis and decreased upon 240−380 nm irradiation and upon annealing to 20 K. The bands shift to 803.7 and 764.0 cm^{-1} with D_2, giving 1.404 and 1.399 H/D isotopic ratios. Experiments with HD in argon produced two median bands at 1098.0 and 782.5 cm^{-1}, as shown in Figure 7. These isotopic patterns are characteristic of the ν_1 and ν_3 modes of a metal dihydride. Two sets of absorptions were observed for BaH_2 in solid neon: a sharp pair at 1131.3 and 1067.9 cm^{-1} and a strong, broader feature at 1027.6 cm^{-1}. Neon/D_2 counterparts at 807.7, 764.9, and 732.7 cm^{-1} define 1.401, 1.396, and 1.402 H/D ratios and suggest that the sharp 1131.3 and 1067.9 cm^{-1} bands are due to the ν_1 and ν_3 modes of isolated BaH_2 in solid neon and the broader band is due to the ν_3 mode of a $(H_2)_nBaH_2$ complex. The neon/HD experiment provides sharp intermediate bands at 1100.4 and 785.5 cm^{-1} that confirm the above ν_1 and ν_3 assignments, and gives additional broad 1050, 1019, and 751 cm^{-1} bands. The weaker 1050 and 751 cm^{-1} bands are BaHD counterparts for the dihydrogen complex, but the stronger 1019 cm^{-1} absorption

results from isotopic exchange with coordinated HD where $(HD)_nBaHD$ rearranges to $(HD)_{n-1}(D_2)BaH_2$ during relaxation. This exchange is taken to the extreme for Ba in pure HD where the only band observed at 1024.5, 1014.4 cm^{-1} is due to the rearranged complex $(HD)_n(D_2)BaH_2$ species. This H/D exchange arises because $(D_2)BaH_2$ has a lower computed zero point energy than (HD)BaHD (by almost 1 kcal/mol). Similar dihydrogen/dihydride isotopic exchange processes have been found with other metals.[9]

In solid hydrogen, the pattern found for Ca and Sr continued for Ba, and a strong 1007.6 cm^{-1} band was observed along with a weaker 1064.6 cm^{-1} partner: These bands are due to the ν_3 and ν_1 modes for BaH_2 in solid hydrogen, which is in fact a $(H_2)_nBaH_2$ complex. Broad 4042 and 3966 cm^{-1} absorptions track with the latter bands upon irradiation and are due to the H_2 ligands: Counterpart D_2 bands at 2903 and 2852 cm^{-1} and HD bands at 3525 and 3453 cm^{-1} are observed. The corresponding bands for $(H_2)_nSrH_2$ are 4090 and 4060 cm^{-1}, and the single such band for $(H_2)_nCaH_2$ appeared at 4071 cm^{-1}. These shifts in the H−H frequency from the *p*-H_2 value (4153 cm^{-1})[15] show that the bonding interaction of H_2 ligands increases as $CaH_2 \rightarrow SrH_2 \rightarrow BaH_2$. Similar absorptions were observed for $(H_2)_nMgH_2$ at 4139 and 4114 cm^{-1}.[11b]

Our theoretical frequency calculations support the identifications of CaH_2, SrH_2, and BaH_2. At the B3LYP level of theory, all three metal dihydrides are calculated to be bent and ν_3 modes are predicted at 1254.1 cm^{-1} (CaH_2), 1159.9 cm^{-1} (SrH_2), and 1102.1 cm^{-1} (BaH_2), which are only 2−3% higher than the argon matrix values. The MP2 calculations give very similar frequencies at 1264.8 cm^{-1} (CaH_2), 1141.4 cm^{-1} (SrH_2), and 1101.3 cm^{-1} (BaH_2). B3LYP calculations gave the bent structures for all three dihydrides, while MP2 calculations predicted a linear structure for CaH_2 and bent structures for SrH_2 and BaH_2. The critical problem is that these molecules have extremely flat bending potentials, which results in different bond angles for the same molecule optimized by different theoretical methods. However, the calculated bond lengths correlate well with experimental M−H stretching frequencies.

The insertion reactions of ground-state Ca, Sr, and Ba into H_2 are endothermic by 1.5 (CaH_2), 9.1 (SrH_2), and 0.1 (BaH_2) kcal/mol from B3LYP calculations, but excited metal atoms will insert into H_2. In the case of Ca and Sr in solid H_2, $\lambda > 470$ nm irradiation, which is more than adequate to excite the $^3P_0$ state,[30] does not form dihydrides but $\lambda > 380$ nm irradiation produces strong dihydride absorptions. The latter easily accesses the ^1P states,[31] which clearly react with H_2. In the case of Ba, $\lambda > 530$ nm irradiation initiates the reaction, but $\lambda > 470$ nm light is even more efficient, and the Ba(^1P) state appears to be the reactive species. With $\lambda > 290$ nm irradiation, these metal atoms must be photoexcited to the ^1P state and they then react with H_2 to give MH_2 molecules that are relaxed and trapped in the low-temperature matrix. A similar reaction mechanism was observed for Mg and Be with H_2.[10,11]

$HCaH_2CaH$. Two broad bands at 1057 and 874 cm^{-1} track together in Ca atom reactions with H_2 in solid argon. As shown in Figure 1, these bands were barely observed after deposition but they increased upon near-UV photolysis. The latter bands are much stronger relative to CaH_2 with higher laser energy. The locations in the bridged Ca−H−Ca stretching region suggest the CaH_2 dimer assignment in comparison with infrared spectra of Mg_2H_4 and Be_2H_4 in our earlier works.[10,11] With D_2 in argon, these bands shift to 771 and 634 cm^{-1}, respectively. The neon experiments gave very clear absorptions for the CaH_2 dimer: Strong bridged Ca−H−Ca stretching modes were observed at 1072 and 878 cm^{-1}, which are in concert with argon−neon shifts for typical species.[27] The Ca−H stretching mode is split into four bands at 1224.3, 1221.0, 1217.3, and 1213.5 cm^{-1} because of matrix sites. The deuterium counterpart bands were observed at 785 and 634 cm^{-1} (Ca−D−Ca stretching) and 891.5, 889.2, 886.6, and 883.6 cm^{-1}(Ca−D stretching)

In solid normal hydrogen, the bands at 1215.4, 1073, and 877 cm^{-1} show the same photochemistry; these bands appeared upon $\lambda > 470$ nm photolysis and increased 2-fold upon $\lambda > 380$ nm irradiation. In solid normal deuterium, the lower two bands shift to 783 and 631 cm^{-1} and the upper band is masked by CaD_2.

Determination of the most stable structure of the CaH_2 dimer is not straightforward, since the double-bridged (DB) D_{2h} form is only 1.4 kcal/mol lower in energy than the triple-bridged (TB) C_{3v} form based on early MP2 calculations.[20] We used the B3LYP functional with a large basis set (6-311++G(3df,3pd)) to recalculate these two conformers and found the C_{3v} form (triple-bridged $HCaH_3Ca$) is the more stable structure for the CaH_2 dimer. However, the D_{2h} form is only 1.2 kcal/mol higher in energy, but the order again is reversed with the MP2 method. The calculated strongest IR-active frequencies at 1257.5 cm^{-1} (Ca−H stretching) and 1094.6 and 902.0 cm^{-1} (CaH_3Ca stretching) for the C_{3v} form overestimate the neon Ca_2H_4 frequencies by 2.7, 2.0, and 2.8%, respectively. However, the calculated IR-active frequencies of the D_{2h} form at 1291.6 cm^{-1} (Ca−H stretching) and 1087.9 and 900.3 cm^{-1} (CaH_2Ca stretching) are almost as close to the observed bands. Mixed H/D isotopic experimental and theoretical data are needed for structure determination.

Experiments with pure HD and HD in neon gave diagnostic bands for identification of the CaH_2 dimer. In solid neon, HD substitution gave new bands at 1222, 1164, 1037, 876, 808, 785, and 664 cm^{-1}. Pure solid HD yielded the same bands with ±3 cm^{-1} deviations. Starting with CaHD, the $HCaH_3Ca$ conformer has two substituted forms, namely, $HCaHD_2Ca$ and $DCaDH_2Ca$, and for the $HCaH_2CaH$ structure, there are three forms (HCaHDCaD, $HCaD_2CaH$, and $DCaH_2CaD$), and all of these have been calculated. First of all, the 1222 and 876 cm^{-1} bands are due to terminal Ca−H and Ca−D stretching modes and are compatible with either structure.

The strongest mode calculated for both mixed isotopic TB molecules is 849 cm^{-1}, and the next strongest modes are 1094 and 1143 cm^{-1}. No bands are observed in the region near these calculated frequencies. In fact, the strong computed band of $DCaH_2DCa$ at 1094 cm^{-1} is coincident with this mode for $HCaH_3Ca$, and the strongest band observed for the all-H species at 1072 cm^{-1} is *not* present in the HD experiment. This evidence casts doubt on the TB structure for the Ca_2H_4 species. However, the strongest bands for HCaHDCaD are computed at 1041 and 669 cm^{-1}, and the strongest observed HD product absorptions are 1037 and 664 cm^{-1}, which is the same agreement found for the all-H and all-D species. The weaker 742 cm^{-1} band is probably due to the $HCaD_2CaH$ species, and the 808 cm^{-1} band is likely due to the $DCaH_2CaD$ structure, but we cannot be certain due to band masking in other spectral regions.

Xiao et al. assigned four absorptions to the $HCaH_2CaH$ molecule in solid krypton, and two of these, 1024 and 890 cm^{-1}, are in accord with earlier[20] and present calculations for the Ca−H−Ca bridge stretching modes. These two krypton matrix absorptions are also in agreement with our argon matrix (1057 and 874 cm^{-1}) and neon matrix (1073 and 878 cm^{-1}) observations for $HCaH_2CaH$. It appears that the more intense b_{1u} mode

parallel to the HCa−CaH axis is more vulnerable to perturbation than the less intense b_{2u} motion perpendicular to this axis.

$HSrH_3Sr$. New bands at 1047, 979, 813, 719, and 556 cm^{-1} were produced in solid neon with Sr and H_2 reaction upon $\lambda > 380$ nm photolysis along with SrH_2. The SrH_2 dimer structure must be considered: The DB form in D_{2h} symmetry has one imaginary frequency and distorts to C_{2h}, but the TB form is the minimum energy structure with both calculations (Table 5). With D_2 in neon, these bands shift to 752, 718, 581, and 521 cm^{-1}, and the bending mode falls below our measurement region. Although the all-H and all-D bands could fit the C_{2h} isotopic frequencies, the HD data and the low-frequency bending mode require the C_{3v} form. The bending mode is calculated at 570 cm^{-1} (C_{3v}) or 448 cm^{-1} (C_{2h}): Clearly, the 556 cm^{-1} band is appropriate for the C_{3v} triple-bridged structure.[20] With HD in neon, two triplet bands at 1037, 1006, and 967 cm^{-1} in the Sr−H−Sr stretching region and at 755, 738, and 720 cm^{-1} in the Sr−D−Sr stretching region are diagnostic for $Sr-H_2D-Sr$ and $Sr-HD_2-Sr$ subunits. Hence, the HD band splitting supports the $HSrH_3Sr$ assignment.

The absorptions of $HSrH_3Sr$ were also observed in solid hydrogen at 1121, 1041, 974, 808, and 556 cm^{-1}, which are only a few wavenumber red shifts in comparison with the neon values. The $DSrD_3Sr$ bands in solid D_2 appeared at 747, 717, and 577 cm^{-1}.

$HBaH_3Ba$. The irradiation that formed BaH_2 in solid neon also produced new 881 and 758 cm^{-1} absorptions. The 881 cm^{-1} band shifted to 626 cm^{-1} with D_2 substitution (H/D ratio 1.407). Similar bands were observed in other matrixes, and diagnostic HD counterparts were observed in solid argon. Our calculations and the previous work[20] find the TB structure $HBaH_3Ba$ to be the global minimum energy structure. The strongest absorptions are predicted at 925 and 771 cm^{-1} for the C_{3v} structure at the B3LYP level, which supports our assignment of the 881 and 758 cm^{-1} bands to the BaH_2 dimer in the $HBaH_3Ba$ structure. Furthermore, the higher energy C_{4v} structure has very strong bands predicted at 944 and 835 cm^{-1}, which do not fit the experimental frequencies nearly as well.

The C_{3v} structure is confirmed by the HD experiment with slightly higher laser energy using argon samples where two broad 887, 860 cm^{-1} and 686, 664 cm^{-1} bands were observed in addition to BaHD and its clusters with HD. The strongest two bands of $HBaHD_2Ba$ and $DBaH_2DBa$ are computed at 969, 740 cm^{-1} and 925, 707 cm^{-1}, respectively (see Table 6). These bands bracket the strongest band calculated for $HBaH_3Ba$ at 926 cm^{-1} and are just above the strongest band computed for $DBaD_3Ba$ at 657 cm^{-1}. Notice that the observed HD bands have the same relationship with the strongest observed band (875 cm^{-1}) for $HBaH_3Ba$ and for $DBaD_3Ba$ (627 cm^{-1}).

Solid Hydrides. Solid hydride films have been formed in this laboratory upon sublimation of the hydrogen matrix and association of the trapped hydride molecules. We have observed solid aluminum and magnesium hydrides with infrared absorptions very similar to those of the pure solid.[11,12] The MgH_2 molecule is stable enough to be observed in the gas phase,[34] and the association of MgH_2 molecules forms the same polymeric MgH_2 solid as that produced from the elements at high temperature.[11] The CaH_2 molecule is less stable,[2] and upon evaporation of the solid H_2 matrix, CaH_2 and Ca_2H_4 absorptions are replaced by a broad 1200−600 cm^{-1} band recorded at 10−30 K, which decreases upon warming to 295 K, leaving a weak 1050 cm^{-1} band with a 1100 cm^{-1} shoulder. This is probably due to a Ca−H−Ca bridge stretching mode in a CaH_2 polymer film, as it is near our 1070 cm^{-1} absorption for $HCaH_2CaH$ and 128 mev (1030, 1090 cm^{-1}) features in the inelastic neutron scattering spectrum of solid calcium hydride.[1c] On the other hand, the SrH_2 and BaH_2 molecules are less stable,[2] and upon sublimation of the H_2 matrix and loss of these MH_2 molecules and their HMH_3M dimers, we find no solid hydride absorptions. We note that the strongest bridge-bond stretching mode in our M_2H_4 molecules (M = Ca, Sr, and Ba) is within 15 cm^{-1} of the highest frequency absorption in the infrared spectra of the solid MH_2 compounds.[1a]

Bonding of Group 2 Metal Hydrides. The group 2 metal dihydrides are the simplest MX_2 compounds, and their structure determination is one of "the most intriguing problems of modern inorganic chemistry",[32] since their structures have been controversial for a long period of time.[8] The dihydrides of beryllium and magnesium are linear, as confirmed from infrared spectra of both gas-phase[33,34] and matrix samples.[10,11] Similarly, linear dihalides of beryllium and magnesium were found from infrared spectroscopy[35] and electron diffraction.[36] The linear dihydrides and dihalides of beryllium and magnesium are in excellent agreement with theoretical calculations without any exception.[37] For most molecules trapped in solid matrixes, a slightly lower frequency is found in solid argon and the solid hydrogen and neon values fall in the middle, and the gas-phase value is still higher.[9,27] The ν_3 absorption of BeH_2 at 2159.1 cm^{-1} in solid argon, 2165.0 cm^{-1} in solid hydrogen, 2170.9 cm^{-1} in solid neon, and 2178.9 cm^{-1} in the gas phase is a case in point.[10,33] A similar trend is found for MgH_2 and the group 12 metal dihydrides ZnH_2, CdH_2, and HgH_2.[11,34,38,39]

However, the ν_3 mode of CaH_2 was observed at 1202.8 cm^{-1} in solid neon and at 1196.9 cm^{-1} in solid hydrogen, but surprisingly, this mode is higher at 1216.3 cm^{-1} in solid argon. Furthermore, the very weak ν_1 mode of CaH_2 was observed in argon, indicating a bent structure, but the symmetric mode was not observed in solid neon and hydrogen, and a more nearly linear structure is suggested. Obviously, interaction between the more polarizable argon matrix and CaH_2 sustains the bent structure.

We report here the first experimental observations of SrH_2 and BaH_2. Similar but even larger matrix shifts were observed for SrH_2 than for CaH_2. In solid neon, the ν_3 mode of SrH_2 appeared at 1100.4 cm^{-1} and in solid hydrogen at 1093.5 cm^{-1}, but this mode is also higher at 1132.4 cm^{-1} in solid argon where the ν_1 mode was observed at 1202.1 cm^{-1} with greater intensity relative to ν_3 than that found for CaH_2. This 32 cm^{-1} blue shift from neon to argon for the ν_3 mode of SrH_2 is very unusual, and it suggests a structure change of increasing H−Sr−H angle upon going from the argon to neon matrix environment. Barium dihydride presents almost the same situation: The ν_3 fundamental is 1068.6 cm^{-1} in argon and 1007.6 cm^{-1} in solid hydrogen. The solid hydrogen frequencies are really due to $(H_2)_nSrH_2$ and $(H_2)_nBaH_2$ complexes, which will have different valence angles from the argon complexes, that is, the molecules trapped in solid argon and the isolated molecules.

The covalent bonding in heavy alkaline-earth metal hydrides must involve d-orbitals.[4,20] The solid matrix can induce metal cation polarization and enhance the d-orbital participation. The CaH_2 and SrH_2 molecules have very shallow bending potentials, and the barrier to attain linearity for CaH_2 is <1 kcal/mol.[5] Thus, these molecular shapes can vary upon interaction with the surrounding matrix, and small induced dipole moments may cause equilibrium structure changes. As we know, the solid argon matrix is more polarizable, in which CaH_2 and SrH_2 are clearly bent, while in solid neon these molecules are more nearly

TABLE 7: Absorptions of the MH and MH_2 (ν_3 Mode) Molecules in Solid Argon, Hydrogen, Neon, and the Gas Phase and Comparison with Theoretical Calculations

species	argon	hydrogen	neon	gas phase[a]	B3LYP	MP2
BeH	1971.1	1978.2	1983.6	1986.6	2061.0	2111.9
MgH	1422.1	1427.1	1431.3	1431.4	1461.6	1556.2
CaH	1262.0	1255.1	1258.2	1260.1	1292.9	1307.2
SrH	1174.6	1166.7	1171.1	1172.8	1184.2	1179.2
BaH	1132.5			1139.2	1155.4	1167.4
ZnH	1493.9	1495.9	1497.7	1496.5	1511.9	
CdH	1339.4	1340.4	1340.6	1336.9	1366.1	
HgH		1205.7		1203.2	1226.6	
BeH_2	2159.5	2165.0	2170.9[b]	2178.9	2262.8	2285.4
MgH_2	1571.9	1569.5	1574.0[c]	1588.7	1637.3	1659.4
CaH_2	1216.3[d]	1196.9	1203.1		1254.1	1264.8
SrH_2	1132.4[e]	1099.5	1100.4		1159.9	1141.4
BaH_2	1068.6[f]	1007.6	1027.6		1102.1	1101.3
ZnH_2	1870.2	1875.6	1880.8		1930.6	
CdH_2	1753.5	1758.1	1764.2		1807.3	1791.8
HgH_2	1895.3	1902.2	1918.8		1923.5	1948.5

[a] Gas-phase data from refs 2, 21, 24, 26, 33, 34, 38, 39, and 41 and references therein. [b] Reference 10. [c] Reference 11. [d] ν_1 mode observed at 1289.7 cm^{-1}. [e] ν_1 mode observed at 1202.1 cm^{-1}. [f] ν_1 mode observed at 1128.6 cm^{-1}.

linear. Note that the bent BaH_2 molecule is trapped in both solid argon and neon.

Xiao et al. estimated the H−Ca−H valence angle in solid krypton and xenon as 168 ± 4° using the well-known intensity relationship for the ν_3 (b_2) and ν_1 (a_1) absorptions of a symmetrical triatomic molecule.[3,40] We find a 70 ν_3/ν_1 intensity ratio for CaH_2 in solid argon, which gives a 166° estimate for the CaH_2 valence angle and supports the Rice group estimate. Furthermore, the more bent SrH_2 and BaH_2 molecules exhibit smaller 9.5 and 4.5 ν_3/ν_1 intensity ratios, which give 144 and 130° valence angles, respectively, for SrH_2 and BaH_2. These experimental estimates are very approximate, but when compared with the theoretical valence angles in Tables 4−6 for CaH_2 (143°, 180°), SrH_2 (124°, 140°), and BaH_2 (113°, 119°), a clear trend emerges. Finally, the sharp bands at 1131.3 and 1067.9 cm^{-1} for isolated BaH_2 in solid neon shift only 1−3 cm^{-1} from the argon matrix values and exhibit approximately the same relative intensity. We conclude that BaH_2 has essentially the same 125 ± 10° valence angle in solid argon and neon.

It is interesting to compare the alkaline-earth metal dihydrides with the d^{10} shell metal dihydrides. The metal−hydrogen stretching frequencies of ZnH_2, CdH_2, and HgH_2 are listed in Table 7. Although the gas-phase values are not available for the group 12 metal dihydrides, the argon, neon, and hydrogen values exhibit the usual order,[9,38,39] indicating that interactions between the matrix host and guest molecules is straightforward. The same is found for the ZnH, CdH, and HgH diatomic molecules.[39,41]

It is also interesting to compare the most stable structures of the alkaline-earth metal dihydride dimers. The Be_2H_4, Mg_2H_4, and Ca_2H_4 molecules favor D_{2h} structures with double-bridged M−H−M bonds that are confirmed through infrared spectra with HD substitution in solid hydrogen, neon, and argon. However the C_{3v} conformer with triple-bridged M−H−M bonds is the most stable structure for Sr_2H_4 and Ba_2H_4. Here, d-orbital participation in the bonding is extremely important.[20]

Acknowledgment. We gratefully acknowledge support for this work from N.S.F. grants CHE 00-78836 and CHE 03-52487 and the contributions of S. P. Willson, T. J. Tague, and M. Kaupp on early experiments and calculations.

References and Notes

(1) (a) Maeland, A. *J. Chem. Phys.* **1970**, *52*, 3952. (b) Wells, A. F. *Structural Inorganic Chemistry*; Clarendon Press: Oxford, U.K., 1975. (c) Morris, P.; Ross, D. K.; Ivanov, S.; Weaver, D. R.; Serot, O. *J. Alloys Compd.* **2004**, *363*, 85.

(2) Shayesteh, A.; Walker, K. A.; Gordon, I.; Appadoo, D. R. T.; Bernath, P. F. *J. Mol. Struct.* **2004**, *695*−*696*, 23.

(3) Xiao, Z. L.; Hauge, R. H.; Margrave, J. L. *High Temp. Sci.* **1991**, *31*, 59.

(4) Kaupp, M.; Schleyer, P. v. R.; Stoll, H.; Preuss, H. *J. Chem. Phys.* **1991**, *94*, 1360.

(5) Bytheway, I.; Gillespie, R. J.; Tang, T. H.; Bader, R. F. W. *Inorg. Chem.* **1995**, *34*, 2407.

(6) Fujii, T. S.; Iwata, S. *Chem. Phys. Lett.* **1996**, *251*, 150.

(7) Szentpaly, L. *J. Phys. Chem. A* **2002**, *106*, 11945.

(8) (a) Kaupp, M. *Angew. Chem., Int. Ed.* **2001**, *40*, 3534. (b) Hargittai, M. *Chem. Rev.* **2000**, *100*, 2233.

(9) Andrews, L. *Chem. Soc. Rev.* **2004**, *33*, 123.

(10) (a) Tague, T. J., Jr.; Andrews, L. *J. Am. Chem. Soc.* **1993**, *115*, 12111 (BeH_2). (b) Wang, X.; Andrews, L. Manuscript in preparation $(BeH_2)_n$.

(11) (a) Tague, T. J., Jr.; Andrews, L. *J. Phys. Chem.* **1994**, *98*, 8611 (MgH_2). (b) Wang, X.; Andrews, L. *J. Phys. Chem. A*, in press (Mg_2H_4).

(12) (a) Andrews, L.; Wang, X. *Science* **2003**, *299*, 2049 (Al_2H_6). (b) Wang, X.; Andrews, L.; Tam, S.; DeRose, M. E.; Fajardo, M. *J. Am. Chem. Soc.* **2003**, *125*, 9218 (Al_2H_4). (c) Andrews, L.; Wang, X. *J. Phys. Chem. A* **2004**, *108*, 4202 (Al_2H_6). (d) Andrews, L.; Wang, X. *J. Am. Chem. Soc.* **2002**, *124*, 7280 (BH_4).

(13) (a) Andrews, L.; Wang, X. *Angew. Chem., Int. Ed.* **2004**, *43*, 1706. (b) Wang, X.; Andrews, L. *J. Phys. Chem. A* **2003**, *107*, 11371 (Ga + H_2). (c) Wang, X.; Andrews, L. *J. Phys. Chem. A* **2004**, *108*, 3396 (Tl + H_2). (d) Wang, X.; Andrews, L. *J. Phys. Chem. A* **2004**, *108*, 4440 (In + H_2).

(14) Andrews, L.; Citra, A. *Chem. Rev.* **2002**, *102*, 885 and references therein.

(15) (a) Wang, X.; Andrews, L. *J. Phys. Chem. A* **2004**, *108*, 1103 (H^-). (b) Andrews, L.; Wang, X. *J. Phys. Chem. A* **2004**, *108*, 3879 (H).

(16) Andrews, L.; Yustein, J. T.; Thompson, C. T.; Hunt, R. D. *J. Phys. Chem.* **1994**, *98*, 6514.

(17) Andrews, L.; Wang, X. *Rev. Sci. Instrum.* **2004**, *75*, 3039.

(18) Frisch, M. J.; Trucks, G. W.; Schlegel, H. B.; Scuseria, G. E.; Robb, M. A.; Cheeseman, J. R.; Zakrzewski, V. G.; Montgomery, J. A., Jr.; Stratmann, R. E.; Burant, J. C.; Dapprich, S.; Millam, J. M.; Daniels, A. D.; Kudin, K. N.; Strain, M. C.; Farkas, O.; Tomasi, J.; Barone, V.; Cossi, M.; Cammi, R.; Mennucci, B.; Pomelli, C.; Adamo, C.; Clifford, S.; Ochterski, J.; Petersson, G. A.; Ayala, P. Y.; Cui, Q.; Morokuma, K.; Malick, D. K.; Rabuck, A. D.; Raghavachari, K.; Foresman, J. B.; Cioslowski, J.; Ortiz, J. V.; Stefanov, B. B.; Liu, G.; Liashenko, A.; Piskorz, P.; Komaromi, I.; Gomperts, R.; Martin, R. L.; Fox, D. J.; Keith, T.; Al-Laham, M. A.; Peng, C. Y.; Nanayakkara, A.; Gonzalez, C.; Challacombe, M.; Gill, P. M. W.; Johnson, B.; Chen, W.; Wong, M. W.; Andres, J. L.; Gonzalez, C.; Head-Gordon, M.; Replogle, E. S.; Pople, J. A. *Gaussian 98*, revision A.6; Gaussian, Inc.: Pittsburgh, PA, 1998.

(19) (a) Kauffman, J. W.; Hauge, R. H.; Margrave, J. L. *High Temp. Sci.* **1984**, *18*, 97. (b) Milligan, D. E.; Jacox, M. E. *J. Mol. Spectrosc.* **1973**, *46*, 460. Wight, C. A.; Ault, B. S.; Andrews, L. *J. Chem. Phys.* **1976**, *65*, 1244.

(20) Kaupp, M.; Schleyer, P. v. R. *J. Am. Chem. Soc.* **1993**, *115*, 11202.

(21) Huber, K. P.; Herzberg, G. *Constants of Diatomic Molecules*; Van Nostrand: Princeton, NJ, 1979.

(22) Petitprey, D.; Lemoine, B.; Demuynck, C.; Destombes, J. L.; Macke, B. *Chem. Phys.* **1989**, *91*, 4462.

(23) Forum, C. I.; Pickett, H. M. *J. Mol. Spectrosc.* **1993**, *159*, 329.

(24) Gasmi, K.; Al-Tuwirqi, R. M.; Skowronek, S.; Telle, H. H.; Ureña, A. G. *J. Phys. Chem. A* **2003**, *107*, 10960.

(25) Forum, C. I.; Oh, J. J.; Cohen, E. A.; Pickett, H. M. *J. Mol. Spectrosc.* **1994**, *163*, 339.

(26) Walker, K. A.; Hedderich, H. G.; Bernath, P. F. *Mol. Phys.* **1993**, *78*, 577.

(27) Jacox, M. E. *Chem. Phys.* **1994**, *189*, 149.

(28) Bytheway, I.; Wong, M. W. *Chem. Phys. Lett.* **1998**, *282*, 219.

(29) The *G* matrix elements for the symmetric and antisymmetric modes of an MH_2 group are different: $G_{sym} = \mu H + \mu M + \mu M \cos\alpha$, and $G_{antisym} = \mu H + \mu M - \mu M \cos\alpha$, where μ is the reduced (i.e., inverse) mass. Thus, for $90° < \alpha < 180°$, the symmetric mode has less metal and hence more H participation.

(30) Moore, C. E. *Atomic Energy Levels*; National Bureau of Standards, Circular 467; U.S. Department of Commerce: Washington, DC, 1952.

(31) Andrews, L.; Duley, W. W.; Brewer, L. *J. Mol. Spectrosc.* **1978**, *70*, 41.

(32) Kaupp, M.; Schleyer, P. v. R.; Stoll, H.; Preuss, H. *J. Am. Chem. Soc.* **1991**, *113*, 6012.

(33) (a) Bernath, P. F.; Shayesteh, A.; Tereszchuk, K.; Colin, R. *Science* **2002**, *297*, 1323. (b) Shayesteh, A.; Tereszchuk, K.; Bernath, P. F.; Colin, R. *J. Chem. Phys*. **2003**, *118*, 3622.

(34) Shayesteh, A.; Appadoo, D. R. T.; Gordon, I.; Bernath, P. F. *J. Chem. Phys.* **2003**, *119*, 7785.

(35) (a) Snelson, A. *J. Phys. Chem.* **1966**, *70*, 3208. (b) Lesiecki, M. L.; Nibler, J. W. *J. Chem. Phys*. **1976**, *64*, 871.

(36) (a) Molnar, J.; Marsden, C. J.; Hargittai, M. *J. Phys. Chem.* **1995**, *99*, 9062. (b) Vogt, N.; Girichev, G. V.; Vogt, J.; Girichev, A. G. *J. Mol. Struct.* **1995**, *352*−*353*, 175. (c) Kasparov, V. V.; Ezhov, Y. S.; Rambidi, N. G. *Zh. Strukt. Khim*. **1980**, *21*, 41.

(37) (a) Axten, J.; Trachtman, M.; Bock, C. W. *J. Phys. Chem*. **1994**, *98*, 7823. (b) Ramondo, F.; Bencivenni, L.; Spoliti, M. *THEOCHEM* **1992**, *277*, 171. (c) Dyke, J. M.; Wright, G. *Chem. Phys. Lett.* **1990**, *169*, 138.

(38) Legay-Sommaire, N.; Legay, F. *Chem. Phys. Lett.* **1993**, *207*, 123.

(39) (a) Greene, T. M.; Brown, E.; Andrews, L.; Downs, A. J.; Chertihin, G. V.; Runeberg, N.; Pyykkö, P. *J. Phys. Chem.* **1995**, *99*, 7925 and references therein. (b) Wang, X.; Andrews, L. *J. Phys. Chem. A* **2004**, *108*, 11006.

(40) Ozin, G. A.; McCaffrey, J. G. *J. Phys. Chem.* **1984**, *88*, 645.

(41) Breckenridge, W. H.; Jouvet, C.; Soep, B. *J. Chem. Phys.* **1986**, *84*, 1443.